科学通报 2025 年 第 70 卷 第 2 期: 193 ~ 204
能源电催化专题(II) 论 文
《中国科学》杂志社
SCIENCE CHINA PRESS

微波法快速、原位合成NiFe LDH纳米片阵列用于高效电催化水氧化

王沙沙, 陆徐云, 常亚楠, 李晓萱, 刘影*, 包建春*

南京师范大学化学与材料科学学院, 南京 210023

* 联系人, E-mail: liuyingg@njnu.edu.cn; baojianchun@njnu.edu.cn

2024-01-23 收稿, 2024-04-03 修回, 2024-04-23 接受, 2024-05-09 网络版发表

国家自然科学基金(22102073, 22075147)资助

摘要 氧气析出反应(oxygen evolution reaction, OER)复杂的动力学和高能量势垒严重制约了电解水生产氢能的效率. 基于此, 本工作报道了一种简单、高效的微波合成策略, 可以在碳布表面快速、原位生长层状双金属氢氧化物阵列(layered double hydroxide/carbon cloth, LDH/CC), 用以提升OER性能. 研究发现, 溶剂类型对LDHs的原位生长起着至关重要的作用. 相比于纯水、乙二醇水溶液和季戊四醇水溶液溶剂, 丙三醇水溶液具有适宜的极性, 可以有效调控金属离子的表面能和反应过程中金属离子的成核/迁移, 进而促进LDHs在碳布表面的原位、均匀生长. 与传统的水热法和电沉积法相比, 微波法合成的NiFe LDH/CC具有氧缺陷含量高、电化学活性位点丰富、界面电荷转移电阻低和内在活性高等优点. 以OER为探针反应, 探究并比较了以不同溶剂及合成方法制得的NiFe LDH/CC的电催化性能. 测试表明, 以丙三醇水溶液为溶剂、采用微波法合成的NiFe LDH/CC性能最好, 在100 mA cm^{-2}的过电位(overpotential, η)仅为257 mV(η_{100}), 400 mA cm^{-2}的过电位仅为331 mV(η_{400}), 持续测试100 h后性能仍保持95%, 显著优于以乙二醇水溶液(287和386 mV)、季戊四醇水溶液(309和406 mV)为溶剂的对比样, 以及水热法(279和434 mV)、电沉积法(293和380 mV)合成NiFe LDH/CC的电催化性能. 进一步, 这些性能优于近些年报道的很多过渡金属化合物. 这种微波合成策略不仅适用于NiFe LDH, 还可以原位合成NiMn LDH、CoFe LDH、NiCo LDH, 为高活性LDH的原位、快速合成提供了一种新方法.

关键词 电催化, 氧气析出反应, 微波法, NiFe层状双金属氢氧化物

电催化氧气析出反应(oxygen evolution reaction, OER)是水裂解[1]、燃料电池[2]和金属-空气电池[3]中最重要的半反应之一, 包括四个电子/质子的耦合过程, 涉及*OH、*O和*OOH多个中间体的形成, 导致OER动力学缓慢, 需要较大的过电位才能推动反应的进行[4~7]. 因此, 高活性/稳定性催化剂的设计开发具有重要意义. 虽然RuO_2和IrO_2具有优异的电催化OER性能, 但高昂的价格、稀缺的地球储量限制了其大规模应用[8~10]. 层状双金属氢氧化物(layered double hydroxides, LDHs)具有丰富的地球储量、低廉的使用成本、优异的理化性质、灵活的结构组成和优良的电催化活性, 被认为是先进的电催化剂之一[11~13]. 例如CoFe LDH[14]、MgAl LDH[15]、ZnFe LDH[16]、CuAl LDH[17]和NiFe LDH[18]在储能和能量转换应用中都表现出优异的性能. 其中NiFe LDH因其独特的结构[19]和可调的构型在电催化领域引起了广泛的关注[18,20], 尤其是在电化学OER方面表现出优越的应用潜力[21~23].

LDHs的合成方法多种多样, 如共沉淀法[24]、水热

引用格式: 王沙沙, 陆徐云, 常亚楠, 等. 微波法快速、原位合成NiFe LDH纳米片阵列用于高效电催化水氧化. 科学通报, 2025, 70: 193–204
Wang S S, Lu X Y, Chang Y N, et al. Rapid and *in-situ* synthesis of NiFe LDH nanosheet array using microwave method for efficient electrocatalytic water oxidation (in Chinese). Chin Sci Bull, 2025, 70: 193–204, doi: 10.1360/TB-2024-0090

© 2024《中国科学》杂志社

法[25]、电沉积法[26]、原子层沉积[27]等. 但共沉淀法制得的LDHs结晶性较低, 电子电导率有待进一步提升. 水热法在密闭反应釜中进行, 环境危险系数较高, 耗时长, 且长时间的温度和压力处理导致LDHs的生长速度和化学成分难以准确控制. 电沉积法的放大工艺相对困难, 大面积电沉积可能导致电镀不均匀, 从而影响催化剂的电催化性能[28]. 原子层沉积通常在高温条件下进行, 容易导致LDHs晶体结构破坏或晶格氧失衡; 与此同时, 其沉积速度慢也是不可忽视的问题[29]. 相比之下, 微波法可在短时间内实现快速、均匀加热, 促进晶核的生成和生长, 具有便捷高效、能耗低、用时短等优点[30], 应用前景良好. 虽然目前已有微波辅助合成LDHs的报道[31~33], 但仍局限于粉末状纳米/微米材料[31,34,35], 而利用微波法在基底表面原位生长纳米/微米阵列的方法还未见报道. 相比于粉体材料, 阵列结构具有多重优点, 如有利于电解液扩散、质子传递、电子传输, 以及不需要额外的黏结剂即可直接用于电化学测试等[12,36,37], 因此亟须开发利用微波法原位合成纳米/微米阵列结构的策略.

基于以上调研, 我们报道一种简单、高效的微波合成策略, 可以在碳布(carbon cloth, CC)表面原位生长过渡金属氢氧化物纳米片(NiFe LDH/CC、NiMn LDH/CC、CoFe LDH/CC、NiCo LDH/CC), 其中NiFe LDH/CC表现出最优异的电催化OER性能. 研究发现, 丙三醇水溶液对LDHs纳米片的原位生长起着至关重要的作用. 这主要是因为相比于纯水、乙二醇水溶液和季戊四醇水溶液溶剂, 丙三醇水溶液具有适宜的极性, 可以有效调控金属离子的表面能和反应过程中金属离子的成核/迁移, 有利于LDHs在碳布表面的原位、均匀生长. 系统的光谱学和电化学测试表明, 相比于传统的水热法和电沉积法, 微波法合成的NiFe LDH/CC纳米片阵列具有分布均匀、氧缺陷含量高、电化学活性位点丰富、界面电荷转移电阻低和本征活性高等优点. 因此, 当应用于电催化OER时, 以丙三醇水溶液为溶剂、采用微波法合成的NiFe LDH/CC表现出优异的电催化性能, 在100、200、400 mA cm^{-2}的过电位仅为257 mV(η_{100})、279 mV(η_{200})、331 mV(η_{400}), 显著优于以乙二醇水溶液(287、318和386 mV)、季戊四醇水溶液(309、344和406 mV)为溶剂的对比样, 以及水热法(279、320和434 mV)、电沉积法(293、315和380 mV)合成NiFe LDH/CC的电催化性能. 与此同时, 该催化剂还具有长久的电催化稳定性, 持续测试100 h后性能仍保持95%, 证实了其优异的电催化性能. 这种微波合成策略具有效率高、能耗低、合成产物分布均匀、电催化性能优异等特点, 在能源领域具有良好的拓展应用前景.

1 实验

(i) 材料和试剂. 六水合硝酸镍($Ni(NO_3)_2·6H_2O$, 国药化学试剂有限公司)、七水合硫酸亚铁($FeSO_4·7H_2O$, 国药化学试剂有限公司)、六水合硝酸钴($Co(NO_3)_2·6H_2O$, 成都科龙化工有限公司)、一水合硫酸锰($MnSO_4·H_2O$, 国药集团化学试剂有限公司)、尿素(CH_4N_2O, 国药化学试剂有限公司)、氢氧化钾(KOH, 85%, 国药化学试剂有限公司)、氨水溶液($NH_3·H_2O$, 25wt%~28wt%)、丙三醇(国药化学试剂有限公司)、乙二醇(国药化学试剂有限公司)、季戊四醇(上海化学试剂站)均为分析级, 无需纯化, 直接使用.

碳布预处理: 首先用丙酮/乙醇混合溶液(体积比1/1)超声处理15 min, 以除去表面油渍. 处理后的碳布用去离子水冲洗干净, 浸没于浓HNO_3溶液, 溶剂热110°C反应2 h. 最后, 将碳布用去离子水冲洗干净, 真空干燥备用.

(ii) 催化剂的制备. 称取3 mmol $Ni(NO_3)_2·6H_2O$, 1.5 mmol $FeSO_4·9H_2O$, 24 mmol尿素溶于50 mL去离子水中, 搅拌20 min后加入45 mL丙三醇, 搅拌均匀. 然后将2 cm × 3 cm的碳布浸入上述溶液, 充分浸润后, 将混合液转移至250 mL三颈烧瓶, 在800 W, 100°C的条件下微波照射处理1 h. 反应结束后, 取出碳布, 用去离子水和无水乙醇清洗. 清洗后的碳布在60°C下干燥过夜, 即可得到NiFe LDH/CC.

采用与上述相同的实验方法, 仅将$FeSO_4·9H_2O$替换为$MnSO_4·H_2O$, 合成了NiMn LDH/CC; 仅将$Ni(NO_3)_2·6H_2O$替换为$Co(NO_3)_2·6H_2O$合成了CoFe LDH/CC; 仅将$FeSO_4·9H_2O$替换为$Co(NO_3)_2·6H_2O$合成了NiCo LDH/CC.

(iii) 仪器表征. 采用扫描电子显微镜(scanning electron microscopy, SEM, 加速电压 200 kV, Tescan Mira4)、透射电子显微镜(transmission electron microscopy, TEM, 加速电压200 kV, JEM-200CX, 日本)、高分辨透射电子显微镜(HRTEM, 加速电压200 kV, FEI talos F200X)观察样品形貌和微结构. 采用阳极转靶X射线衍射仪(XRD, D/max 2500VL/PC, Cu Kα激发源, λ = 0.154060 nm, 工作电压45 kV, 电流200 mA, 日本)测

试样品元素组成和物相. 采用X射线光电子能谱(X-ray photoelectron spectroscopy, XPS, 测试管电压和电流分别是12 kV和6 mA, Al Kα激发源, Thermo Scientific)测试样品元素价态, 测试得到的所有数据以C 1s峰(284.8 eV)为标准校正.

(iv) 电化学测试. 在1.0 mol/L KOH水溶液中, 采用CHI 660E电化学工作站(上海晨华仪器有限公司)的三电极系统进行OER的电化学测试. 以碳布(表面原位生长催化剂的碳布)作为工作电极, Hg/HgO电极和石墨棒分别作为参比电极和对电极. 电化学测试前, 首先在1.12~1.72 V(vs. RHE)电位范围内, 通过循环伏安法对催化剂进行预处理. 然后以5 mV s^{-1}的扫描速率, 通过线性扫描伏安法进行极化曲线测试(有IR补偿校正). 除特别说明外, 所有电位均根据能斯特方程(E(vs. RHE) = E(vs. Hg/HgO) + 0.098 + 0.059×pH = E(vs. Hg/HgO) + 0.924)归一化为可逆氢电极(RHE). 电化学双电层电容(C_{dl})的循环伏安测试在非法拉第区域进行, 扫描速率0.02~0.2 V s^{-1}. 电化学阻抗(EIS)测试电位1.49 V(vs. RHE), 频率100 kHz~0.1 Hz. 法拉第效率(Faradaic efficiency, FE)可以根据以下公式计算:

$$FE = \frac{n \times N \times F}{I \times t} \times 100\%,$$

其中, n为产物的实际摩尔数, F为法拉第常数(F = 96485 mol/C), N为反应转移电子数, I是施加的恒定电流, t是反应时间.

2 结果与讨论

2.1 结构表征

NiFe LDH/CC的合成过程如图1(a)所示. 在典型的合成中, 以$Ni(NO_3)_2 \cdot 6H_2O$, $FeSO_4 \cdot 9H_2O$为金属盐前驱体, 尿素水溶液为pH调节试剂, 丙三醇为溶剂, 将碳布浸入上述试剂的混合液中, 100°C微波辐照1 h, 即可在碳布表面原位生长NiFe LDH, 得到NiFe LDH/CC催化剂. 图1(b)为NiFe LDH/CC的X射线衍射图谱(X-ray diffraction, XRD), 其中10.0°、21.2°、34.3°和60.8°处的主衍射峰分别对应NiFe LDH (JCPDS No. 40-215)的(003)、(006)、(012)和(110)晶面. 图1(c)和(d)是NiFe LDH/CC的扫描电子显微镜和透射电子显微镜图像. 由图1(c)可以看出, NiFe LDH/CC呈现三维纳米片阵列结构, 纳米片"聚集体"直径在300~400 nm之间, 表面有明显褶皱, 均匀排列在碳布上, 片层之间存在一定的空隙, 这将有利于电催化反应过程中的质子传递和暴露更多活性位点. 与此同时, 我们还对NiFe LDH/CC进行了高分辨率透射电子显微镜(high resolution transmission electron microscopy, HRTEM)表征(图1(e)). 由图可以观察到明显的晶格条纹, 对应于NiFe LDH的(012)晶面. 插图是NiFe LDH的选区电子衍射(selected area electron diffraction, SAED)图, 其中的衍射环分别对应于NiFe LDH的(110)和(012)晶面, 证实了其NiFe LDH的晶体结构. 此外, 高角度环形暗场扫描透射电镜(high-angle annular dark-field scanning transmission electron microscopy, HAADF-STEM)分析表明, NiFe LDH纳米片较薄, 为电子传输提供了二维路径, 有利于电子的快速传输(图1(f)). 进一步的元素映射图(mapping)(图1(g))说明纳米片中Ni、Fe、O元素均匀分布, 与其NiFe LDH的结构一致.

为了确定NiFe LDH/CC的表面化学状态和电子结构, 我们还对NiFe LDH/CC进行了XPS分析. 图2(a)是NiFe LDH的XPS全谱图, 证实了Ni、Fe和O元素的存在. 图2(b)是Ni 2p的高分辨XPS精细谱, 其中位于855.00、856.93、872.66和874.37 eV的峰分别对应于$Ni^{2+}(2p_{3/2})$、$Ni^{3+}(2p_{3/2})$、$Ni^{2+}(2p_{1/2})$和$Ni^{3+}(2p_{1/2})$. 图2(c)是Fe 2p的XPS精细谱, 可以分为四个信号峰和两个卫星峰, 其中位于713.10和725.87 eV的峰分别对应Fe^{3+}的$2p_{3/2}$和$2p_{1/2}$, 位于710.45和723.05 eV的峰分别对应Fe^{2+}的$2p_{3/2}$和$2p_{1/2}$[22]. 积分计算表明, Fe^{2+}和Fe^{3+}峰面积接近1:1, 表明在NiFe LDH中Fe^{2+}和Fe^{3+}的含量相当. 剩余的两个峰(717.38和733.33 eV)分别对应Ni 2p $2p_{3/2}$和$2p_{1/2}$的卫星峰. 至于O 1s的XPS精细光谱(图2(d)), 可以分为三个峰, 分别归属于金属-氧(metal-oxygen, M-O, 530.03 eV)、氧空位(oxygen vacancy, OV, 531.21 eV), 以及典型的吸附氧(adsorbed oxygen, Abs.O, 532.15 eV). 积分计算表明, NiFe LDH中氧空位的含量约为34%. 这将降低邻近位点的配位数, 有利于羟基在NiFe LDH表面活性位点的吸附, 加强吸附氧的亲电性, 进而促进电催化OER过程.

为了探究NiFe LDH/CC在碳布表面的原位生长机理, 我们进行了一些条件实验. 研究发现, 丙三醇水溶液在LDHs的原位生长过程中发挥重要作用. 如以纯水为溶剂时, 得到的是分散在水溶液中的NiFe LDH纳米片(只有少量原位沉积在碳布表面)(图S1). 这可能是因为金属离子在纯水溶液中的表面能较高, 微波反应过程中这些金属离子将迅速成核、迁移、聚集、生

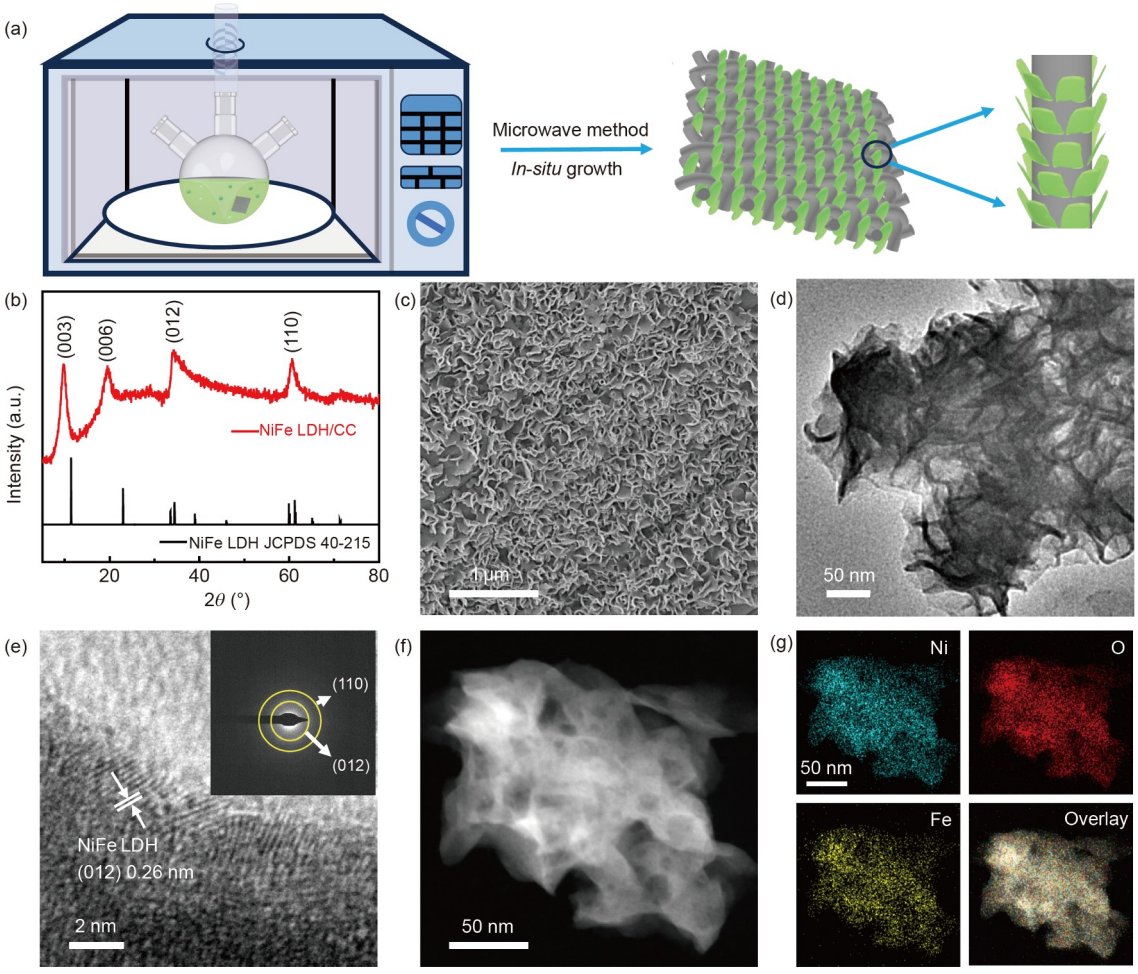


图 1 (网络版彩色)NiFe LDH/CC的合成路线和微结构表征. (a) 微波法合成NiFe LDH/CC的过程示意图. (b) XRD; (c) SEM; (d) TEM; (e) HRTEM(插图是选区电子衍射图); (f) HADDF-STEM; (g) 元素映射图

Figure 1 (Color online) Synthetic route and microstructural characterization of the NiFe LDH/CC. (a) Schematic diagram for the synthesis of the NiFe LDH/CC using a microwave method. (b) XRD; (c) SEM; (d) TEM; (e) HRTEM (the inset is SAED); (f) HADDF-STEM; (g) mapping images

长[38], 因此得到独立分散在水溶液中的NiFe LDH纳米片. 为了控制金属中心的成核位点和生长速率, 我们用季戊四醇水溶液代替纯水, 进行了相同的实验. 结果发现在季戊四醇水溶液中, 实验得到的是原位生长在碳布表面的NiFe LDH/CC(标记为NiFe LDH/CC-PTOL). 这可能是因为相比于纯水溶剂, 季戊四醇水溶液的极性降低, 进而降低了金属核的表面能[39], 促进了金属核在碳布表面成核生长. 图3(a)~(c)是以季戊四醇水溶液为溶剂制得NiFe LDH/CC-PTOL的SEM、TEM和XRD图, 由图可以看出, NiFe LDH/CC-PTOL也呈现三维纳米片阵列结构, 但纳米片尺寸较小(直径约为200 nm), 只有浅浅的一层稀疏排列在碳布纤维表面, 片层之间相对松散. 为了进一步改进纳米片阵列, 我们继续降低溶剂极性, 以乙二醇水溶液和丙三醇水溶液为溶剂进行了实验. 图3(d)~(f)是以乙二醇水溶液为溶剂合成的NiFe LDH/CC(标记为NiFe LDH/CC-EG)的SEM、TEM和XRD图. 由图可以看出, 所得纳米片尺寸较大(直径约为500 nm), 均匀排布在碳布表面, 但片层较厚, 堆叠严重, 这将导致靠近碳布纤维处的纳米片上的活性位点难以有效发挥作用, 也不利于电化学反应过程中的质子传递. 而以丙三醇水溶液为溶剂时, 产物LDHs纳米片尺寸适中, 分散良好, 既能充分暴露电催化活性位点, 又有足够的空隙促进传质, 有利于实现优异的电催化性能. 这些实验结果说明, 溶剂对LDHs在碳布表面的原位生长发挥至关重要的作用, 丙三醇水溶液效果更好. 这可能与其适宜的极性有关. 此外, 为

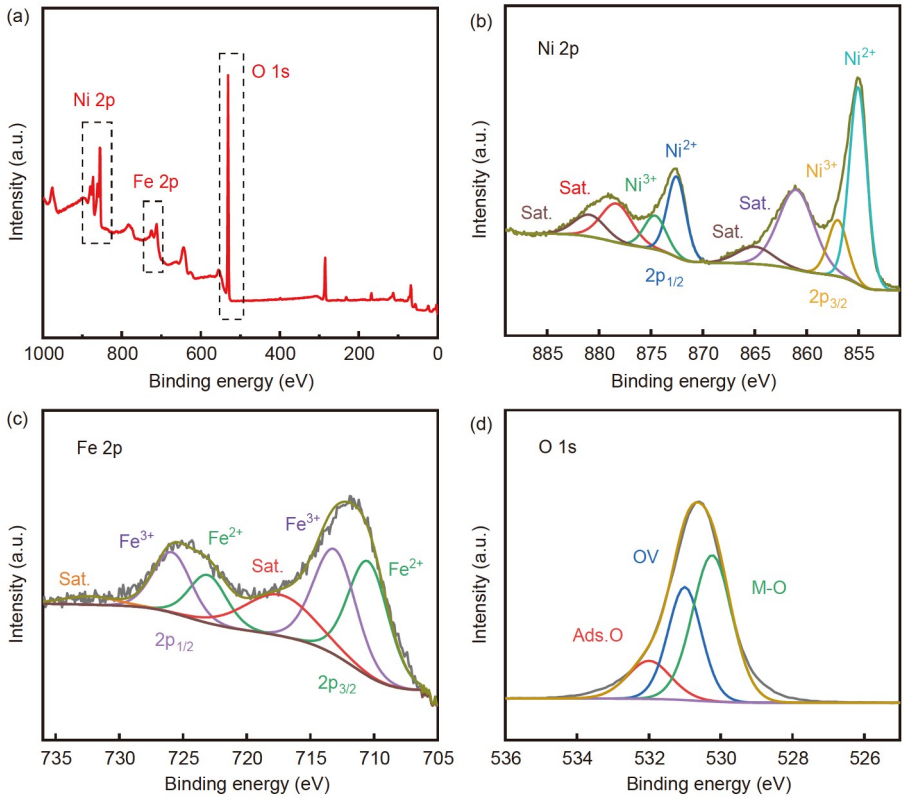


图 2 (网络版彩色)NiFe LDH/CC的XPS谱图. (a) 全谱图; (b) Ni 2p、(c) Fe 2p、(d) O 1s的精细谱图
Figure 2 (Color online) XPS spectra of the NiFe DH/CC. (a) Survey XPS spectrum; fine spectra of (b) Ni 2p, (c) Fe 2p, and (d) O 1s

了进一步探究上述微波合成策略的通用性, 我们还在类似的实验条件下合成了NiMn LDH/CC、CoFe LDH/CC、NiCo LDH/CC(图S2~S4), 证明了微波合成方法的普适性.

2.2 溶剂对NiFe LDH/CC电催化性能的影响

基于上述表征和分析, 溶剂明显影响了NiFe LDH/CC的形貌和微结构, 进而可能影响相关的电催化性能. 因此, 我们对这些催化剂进行了电催化性能测试. 图4(a)是不同溶剂条件下合成的NiFe LDH/CC催化剂的OER线性扫描伏安(linear sweep voltammetry, LSV)曲线. 从图中可以看出, 在碱性条件下(1.0 mol L^{-1} KOH), 丙三醇水溶液中合成的NiFe LDH/CC(即NiFe LDH/CC-Gl)具有明显优于NiFe LDH/CC-EG、NiFe LDH/CC-PTOL的催化电位和电流, 只需要257 mV的过电位(overpotential, η)即可提供100 mA cm^{-2}的电流密度, 而NiFe LDH/CC-EG和NiFe LDH/CC-PTOL和催化剂则分别需要287、309 mV的过电位. 在更大的电流密度下, NiFe LDH/CC-Gl的过电位(η_{200} = 279 mV, η_{400} = 331 mV)也明显小于NiFe LDH/CC-EG(η_{200} = 318 mV, η_{400} = 386 mV)和NiFe LDH-PTOL (η_{200} = 344 mV, η_{400} = 406 mV)(图4(b)), 说明其具有优异的电催化能力. 为了进一步研究溶剂对OER动力学的影响, 我们拟合了Tafel斜率. 如图4(c)所示, NiFe LDH/CC-Gl的Tafel斜率为43.7 mV dec^{-1}, 低于NiFe LDH/CC-EG (52.9 mV dec^{-1})和NiFe LDH/CC-PTOL (54.2 mV dec^{-1}), 说明NiFe LDH/CC-Gl具有更快的反应速率和更低的OER能耗. 这些性能优于许多文献报道的Ni基和Fe基催化剂(图4(d)和表S1). 基于此, 我们测试了NiFe LDH/CC-Gl在100、200和400 mA cm^{-2}下的法拉第效率, 用以评估生产能力和选择性. 如图S5所示, NiFe LDH/CC-Gl在100、200和400 mA cm^{-2}下的法拉第效率分别为98.2%、98.2%、98.7%, 表明NiFe LDH/CC-Gl对OER具有优异的选择性.

为了进一步探究这些催化剂性能差异的原因, 我们进行了电化学阻抗谱(electrochemical impedance spectroscopic, EIS)和双电层电容(double-layer capacitance, C_{dl})测试. 如图4(e)所示, NiFe LDH/CC-Gl的界面

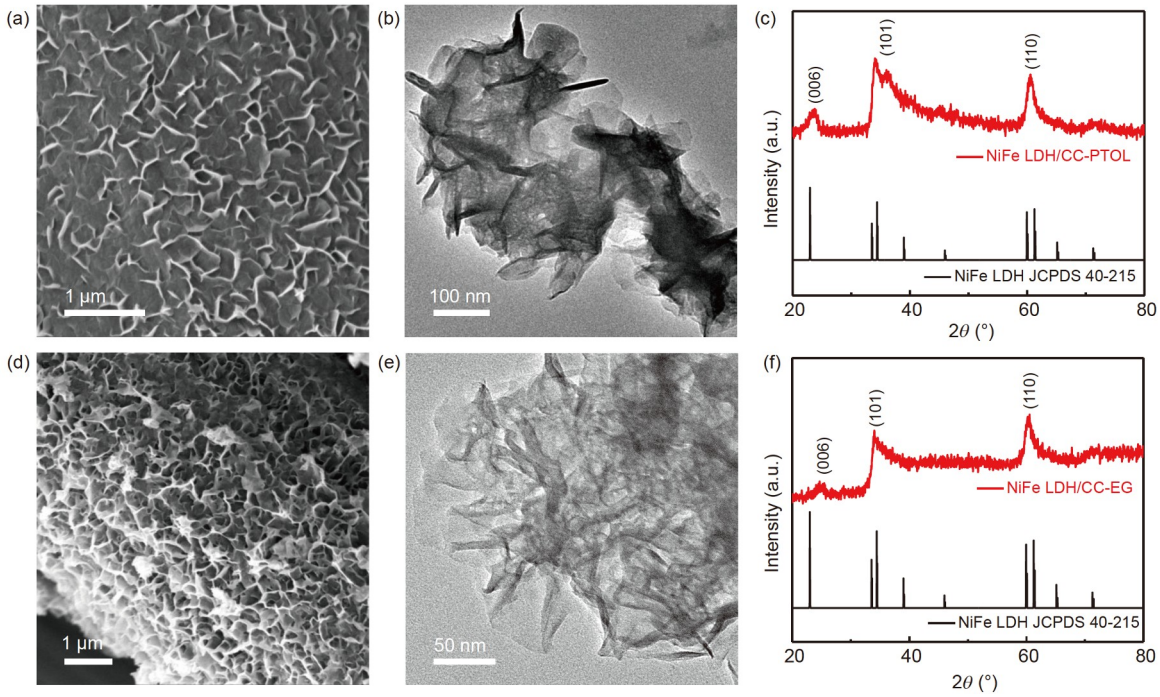


图 3 (网络版彩色)不同溶剂条件下合成NiFe LDH/CC的微结构表征. 以季戊四醇水溶液为溶剂合成的NiFe LDH/CC的(a) SEM、(b) TEM、(c) XRD图像; 以乙二醇水溶液为溶剂合成的NiFe LDH/CC的(d) SEM、(e) TEM、(f) XRD图像

Figure 3 (Color online) Microstructural characterization of the NiFe LDH/CC synthesized under different solvent conditions. (a) SEM, (b) TEM, and (c) XRD images of the NiFe LDH/CC synthesized with pentaerythritol solvent; (d) SEM, (e) TEM, and (f) XRD images of the NiFe LDH/CC synthesized with ethylene glycol solvent

电荷转移电阻(R_{ct})为4.9 Ω, 小于NiFe LDH/CC-EG (6.6 Ω)和NiFe LDH/CC-PTOL(9.2 Ω), 说明以丙三醇为溶剂合成的NiFe LDH/CC-Gl的界面电荷转移阻力更小, 这与其较小的Tafel斜率和改善的反应动力学是一致的. 进一步的C_{dl}测试说明NiFe LDH/CC-Gl的C_{dl}值(2.6 mF cm^{-2})也优于NiFe LDH/CC-EG(1.9 mF cm^{-2})和NiFe LDH/CC-PTOL(1.3 mF cm^{-2})(图4(f)和S6), 说明NiFe LDH/CC-Gl具有更多电化学活性位点. 这可能源于其开放的三维结构和适宜的片层厚度.

2.3 不同方法合成的NiFe LDH/CC的电催化性能

作为对比, 我们通过传统的水热法[40]和电沉积方法[41]合成了与图1(b), (c)类似的、负载在碳布表面的NiFe LDH/CC(图S7和S8). 图5(a)为采用不同方法合成的NiFe LDH/CC的LSV曲线. 由图可知, 微波法合成的NiFe LDH/CC在100、200和400 mA cm^{-2}电流密度下的过电位分别为257、279和331 mV, 明显小于水热法(279、320和434 mV)和电沉积法(293、315和380 mV)合成的NiFe LDH/CC(图5(b)), 表明其能耗更低. 这可能是因为相比于水热法和电沉积法, 微波法合成的NiFe LDH/CC催化剂具有更快的界面电荷转移(图5(c))和更多电催化活性位点(图5(d)和图S9)[42]. 进一步的电子顺磁共振光谱图(electron paramagnetic resonance, EPR)显示, 微波法合成的NiFe LDH/CC的氧缺陷信号峰明显高于水热法和电沉积法合成的NiFe LDH/CC, 说明微波法合成的NiFe LDH/CC具有更多氧缺陷(图5(e)). 这不仅可以提高活性位点数量, 还可以降低周围原子的配位数, 有助于羟基在催化剂活性位点上的吸附, 并改善纳米片的电子结构, 提高其电催化性能[43]. 因此, 我们基于Laviron方程对不同方法合成的NiFe-LDH/CC进行了催化机理研究, 结果如图S10~S12和图5(f)所示. 由图可知, 微波法合成的NiFe LDH/CC的异相电子速率常数Ks(0.19 s^{-1})大于水热法(0.14 s^{-1})和电沉积法(0.13 s^{-1})合成的NiFe LDH/CC, 说明微波法合成的NiFe LDH/CC与羟基中间体的结合强度更强[44].

2.4 NiFe LDH/CC的电催化稳定性

除了活性, 电化学稳定性是评价催化性能的另一个关键指标. 因此, 我们对以丙三醇为溶剂、采用微波法合成的NiFe LDH/CC进行了计时电位测试, 结果如

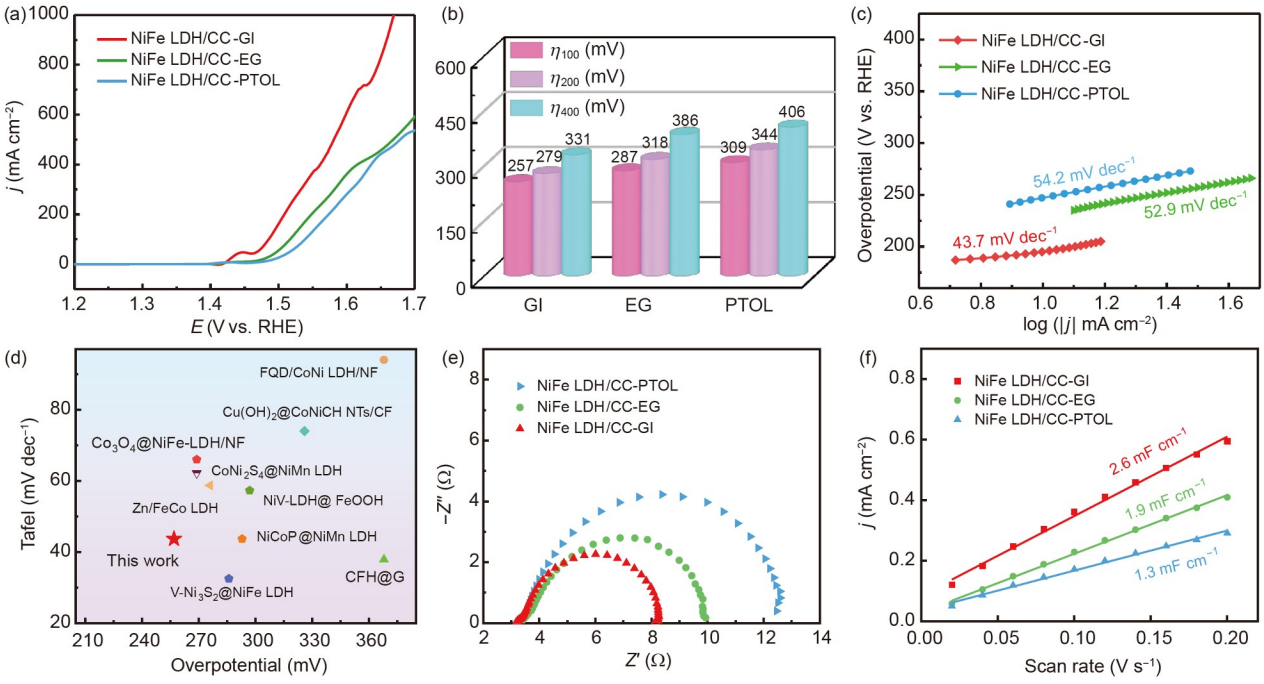


图 4 (网络版彩色)不同溶剂条件下合成的NiFe LDH/CC的电催化OER性能. (a) 线性扫描伏安曲线; (b) 过电位; (c) Tafel斜率; (d) NiFe LDH/CC催化剂和最近报道的一些LDHs的过电位(@100 mA cm^{-2})和Tafel斜率的比较; (e) 电化学阻抗谱图; (f) 电流密度随扫描速率变化的函数图

Figure 4 (Color online) OER performances of the NiFe LDH/CC synthesized with different solvents. (a) LSV curves; (b) overpotentials; (c) Tafel slopes; (d) comparison of overpotentials (@100 mA cm^{-2}) and Tafel slopes of the NiFe LDH/CC catalyst and some recently reported LDHs; (e) EIS spectra; (f) the plots of current densities as a function of scan rates

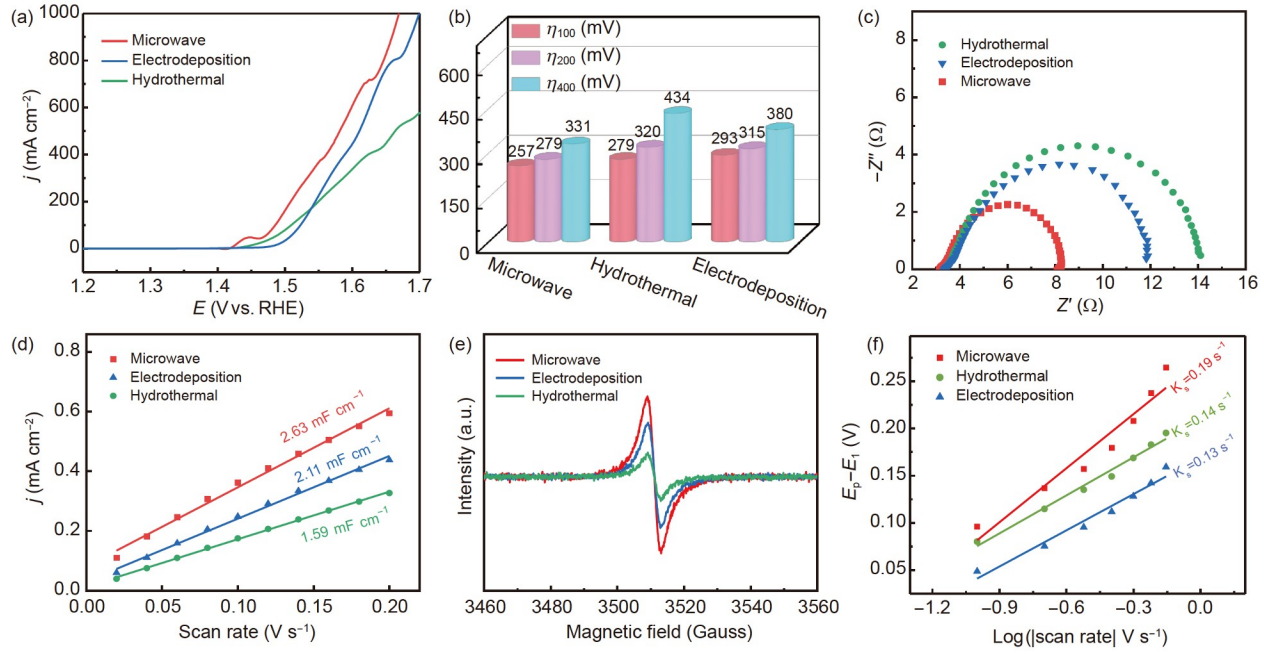


图 5 (网络版彩色)不同方法合成的NiFe LDH/CC的OER性能. (a) 线性扫描伏安曲线; (b) 过电位; (c) 电化学阻抗谱图; (d) 电流密度随扫描速率变化的函数图; (e) 电子顺磁共振光谱图; (f) 异相电子速率常数(E_p为还原电位, $E_{1/2}$为形式电位)

Figure 5 (Color online) OER performances of the NiFe LDH/CC synthesized by different methods. (a) LSV curves; (b) overpotentials; (c) EIS spectra; (d) the plots of current densities as a function of scan rates; (e) EPR spectra; (f) redox constants (E_p is the reduction potential, and $E_{1/2}$ is the formal potential)

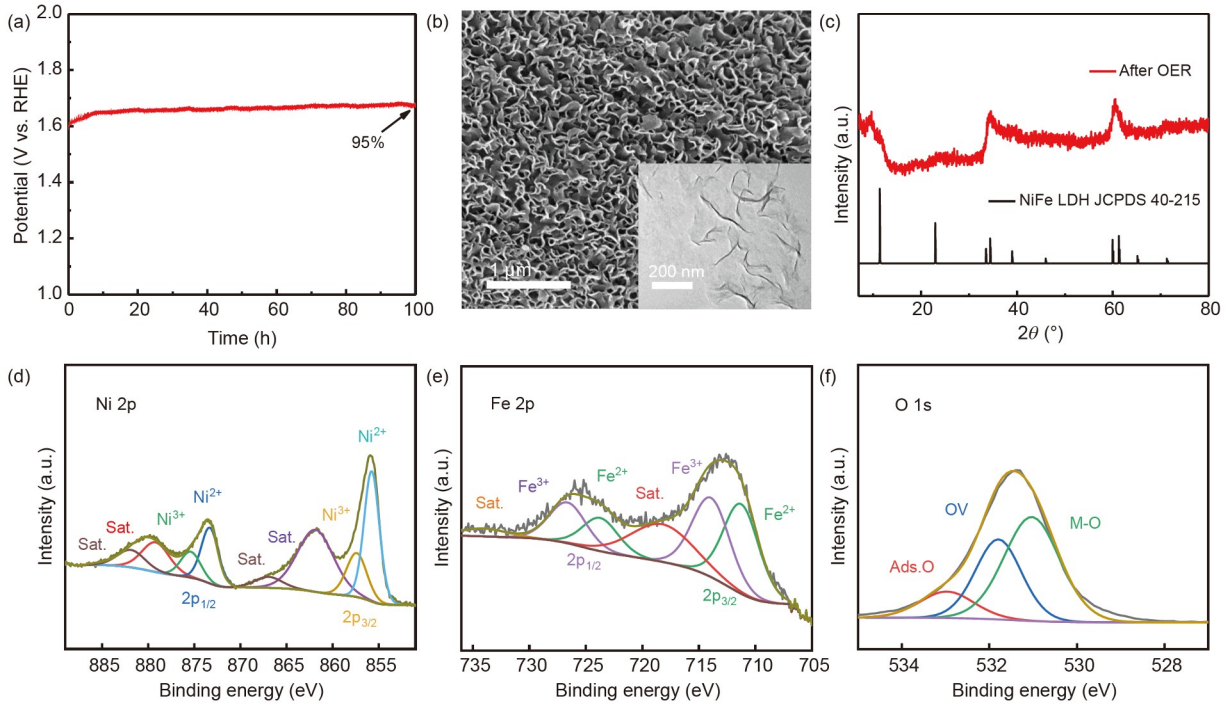


图 6 (网络版彩色)稳定性测试后NiFe LDH/CC的微结构表征. (a) NiFe LDH/CC催化剂的OER稳定性测试曲线; (b) SEM(插图是稳定性测试后NiFe LDH/CC的TEM图); (c) XRD; (d) XPS Ni 2p, (e) Fe 2p, (f) O 1s

Figure 6 (Color online) Microstructural characterization of the NiFe LDH/CC after stability test. (a) OER stability curve of the NiFe LDH/CC catalyst; (b) SEM (the inset is the TEM image); (c) XRD; (d) XPS Ni 2p, (e) Fe 2p, (f) O 1s

图6(a)所示. 在100 mA cm^{-2}恒定电流密度下, 经过100 h的测试后, NiFe LDH/CC的OER性能保持95%, 说明其具有长久的电催化稳定性. 这可能得益于: (1) 相较于使用黏合剂的方法, 原位生长在碳布表面的NiFe LDH和碳布之间的结合更加紧密和牢固, 具有良好的结构稳定性; (2) 在碱性OER中, Fe的存在增强了Ni基氢氧化物的形貌(图6(b))和结构稳定性(图6(c))[4]. 进一步的XPS测试表明, 长期的稳定性测试过程中催化剂仍有部分氧化(图6(d)~(f)). 尽管如此, 其仍可以稳定运行约100 h. 这主要是因为氧化形成的高价态Ni^{3+}和Fe^{3+}也具有一定的电催化OER性能[45,46].

3 结论

综上所述, 本工作采用微波法在碳布表面原位合成了系列过渡金属氢氧化物(NiFe LDH/CC、NiMn LDH/CC、CoFe LDH/CC、NiCo LDH/CC), 其中NiFe LDH/CC表现出最优异的电催化OER性能. 这主要归因于以下因素的综合影响: (1) NiFe LDH/CC的三维开放结构有利于电催化过程中的质子传递和暴露更多活性位点; (2) NiFe LDH/CC含有丰富的氧缺陷, 不仅增加了催化剂吸附氧的亲电性, 有助于羟基的吸附, 还优化了界面电荷分布, 改善了OER电子转移动力学; (3) 自支撑的结构无需额外的黏结剂, 具有良好的导电性和结构完整性, 有利于电化学反应过程中的电荷转移. 相比于传统的水热法和电沉积法, 本工作报道的原位微波合成策略具有简单高效、耗时短、能耗低、产物纳米片分布均匀等优点, 为其他新型、高效多功能电催化剂的原位合成提供了新的路线.

参考文献

1 Su H, Jiang J, Li N, et al. NiCu alloys anchored defect-rich NiFe layered double-hydroxides as efficient electrocatalysts for overall water splitting. Chem Eng J, 2022, 446: 137226

2 Wang H, Yang Y, DiSalvo F J, et al. Multifunctional electrocatalysts: Ru–M (M = Co, Ni, Fe) for alkaline fuel cells and electrolyzers. ACS Catal,

2020, 10: 4608–4616
3 Moloudi M, Noori A, Rahmanifar M S, et al. Layered double hydroxide templated synthesis of amorphous NiCoFeB as a multifunctional electrocatalyst for overall water splitting and rechargeable zinc–air batteries. Adv Energy Mater, 2023, 13: 2203002
4 Lee S Y, Oh H J, Kim M J, et al. Insights into enhanced activity and durability of hierarchical Fe-doped $Ni(OH)_2$/Ni catalysts for alkaline oxygen evolution reaction: *In situ* XANES studies. Appl Catal B-Environ, 2023, 324: 122269
5 Zhao S, Hu F, Yin L, et al. Manipulating electron redistribution induced by asymmetric coordination for electrocatalytic water oxidation at a high current density. Sci Bull, 2023, 68: 1389–1398
6 Chen J, Long Q, Xiao K, et al. Vertically-interlaced NiFeP/MXene electrocatalyst with tunable electronic structure for high-efficiency oxygen evolution reaction. Sci Bull, 2021, 66: 1063–1072
7 Li C, Wang H B, Yang S, et al. Fabrication of vertical graphene-loaded nickel-iron nanoparticles and their oxygen evolution reaction performance (in Chinese). Chin Sci Bull, 2022, 67: 2950–2957 [李晨, 王泓镔, 杨硕, 等. 垂直石墨烯负载镍铁纳米颗粒的制备及其析氧性能. 科学通报, 2022, 67: 2950–2957]
8 Kasian O, Grote J, Geiger S, et al. The common intermediates of oxygen evolution and dissolution reactions during water electrolysis on iridium. Angew Chem Int Ed, 2018, 57: 2488–2491
9 Zhang H, Liu Y, Chen T, et al. Unveiling the activity origin of electrocatalytic oxygen evolution over isolated Ni atoms supported on a N-doped carbon matrix. Adv Mater, 2019, 31: 1904548
10 Zhang J H, Yue Q. Progress on the anode catalysts for proton exchange membrane water electrolysis (in Chinese). Chin Sci Bull, 2022, 67: 2889–2905 [张佳豪, 岳秦. 质子交换膜电解水阳极析氧催化剂. 科学通报, 2022, 67: 2889–2905]
11 Liu L, Cheng M, Yang Z. Improved performance of flower-like ZnAl LDH growing on carbon nanotubes used in zinc–nickel secondary battery. Electrochim Acta, 2018, 277: 67–76
12 Sahoo D P, Das K K, Mansingh S, et al. Recent progress in first row transition metal Layered double hydroxide (LDH) based electrocatalysts towards water splitting: A review with insights on synthesis. Coord Chem Rev, 2022, 469: 214666
13 Chowdhury P R, Medhi H, Bhattacharyya K G, et al. Recent progress in the design and functionalization strategies of transition metal-based layered double hydroxides for enhanced oxygen evolution reaction: A critical review. Coord Chem Rev, 2023, 483: 215083
14 Zhong D, Li T, Wang D, et al. Strengthen metal-oxygen covalency of CoFe-layered double hydroxide for efficient mild oxygen evolution. Nano Res, 2022, 15: 162–169
15 Xu Y N, Li W, Fu H Q, et al. Tuning the microenvironment in monolayer MgAl layered double hydroxide for CO_2-to-ethylene electrocatalysis in neutral media. Angew Chem Int Ed, 2023, 62: e202217296
16 Gautam J, Wang P, Chishti A N, et al. Heterointerface engineering of hierarchically assembling polyoxometalate on zinc/iron layered double hydroxide nanosheet as a remarkable bifunctional electrocatalyst for overall water splitting. J Power Sources, 2023, 581: 233502
17 Iwase K, Hirano T, Honma I. Copper aluminum layered double hydroxides with different compositions and morphologies as electrocatalysts for the carbon dioxide reduction reaction. ChemSusChem, 2022, 15: e202102340
18 Zhou D, Wang S, Jia Y, et al. NiFe hydroxide lattice tensile strain: Enhancement of adsorption of oxygenated intermediates for efficient water oxidation catalysis. Angew Chem Int Ed, 2019, 58: 736–740
19 Sun Z M, Liu Y H, Ding D J, et al. Manganese-doped nickel-iron bimetallic hydroxide catalyst for efficient electrocatalytic oxygen evolution reaction (in Chinese). Chin Sci Bull, 2022, 67: 2423–2430 [孙泽民, 刘宇慧, 丁大杰, 等. 用于高效电催化析氧反应的锰掺杂镍铁双金属氢氧化物催化剂. 科学通报, 2022, 67: 2423–2430]
20 Bodhankar P M, Sarawade P B, Singh G, et al. Recent advances in highly active nanostructured NiFe LDH catalyst for electrochemical water splitting. J Mater Chem A, 2021, 9: 3180–3208
21 Zhai Y, Ren X, Sun Y, et al. Synergistic effect of multiple vacancies to induce lattice oxygen redox in NiFe-layered double hydroxide OER catalysts. Appl Catal B-Environ, 2023, 323: 122091
22 Li X J, Zhang H K, Hu Q, et al. Amorphous NiFe oxide-based nanoreactors for efficient electrocatalytic water oxidation. Angew Chem Int Ed, 2023, 62: e202300478
23 He X, Han X, Zhou X, et al. Electronic modulation with Pt-incorporated NiFe layered double hydroxide for ultrastable overall water splitting at 1000 mA cm^{-2}. Appl Catal B-Environ, 2023, 331: 122683
24 Zhao J, Wang X, Chen F, et al. A one-step synthesis of hierarchical porous CoFe-layered double hydroxide nanosheets with optimized composition for enhanced oxygen evolution electrocatalysis. Inorg Chem Front, 2020, 7: 737–745
25 Chen Q, Ding R, Liu H, et al. Flexible active-site engineering of monometallic Co-layered double hydroxides for achieving high-performance bifunctional electrocatalyst toward oxygen evolution and H_2O_2 reduction. ACS Appl Mater Interfaces, 2020, 12: 12919–12929
26 Ramesh R, Nandi D K, Kim T H, et al. Atomic-layer-deposited MoN_x thin films on three-dimensional Ni foam as efficient catalysts for the electrochemical hydrogen evolution reaction. ACS Appl Mater Interfaces, 2019, 11: 17321–17332

27 Zhang Y, Li L, Du C, et al. Controllable coating NiAl-layered double hydroxides on carbon nanofibers as anticorrosive microwave absorbers. J Mater Sci Technol, 2023, 151: 109–118

28 Salonen L M, Petrovykh D Y, Kolen'ko Y V. Sustainable catalysts for water electrolysis: Selected strategies for reduction and replacement of platinum-group metals. Mater Today Sustain, 2021, 11-12: 100060

29 Li J, Chai G, Wang X. Atomic layer deposition of thin films: From a chemistry perspective. Int J Extrem Manuf, 2023, 5: 032003

30 He W, Qiu H, Meng J, et al. Microwave-assisted synthesis of nano petal-like α-$Ni(OH)_2$/RGO and its electrochemical performance. J Alloys Compd, 2019, 788: 183–190

31 Kuang H, Zhang H, Liu X, et al. Microwave-assisted synthesis of NiCo-LDH/graphene nanoscrolls composite for supercapacitor. Carbon, 2022, 190: 57–67

32 Sreekanth T V M, Dillip G R, Nagajyothi P C, et al. Integration of Marigold 3D flower-like Ni-MOF self-assembled on MWCNTs via microwave irradiation for high-performance electrocatalytic alcohol oxidation and oxygen evolution reactions. Appl Catal B-Environ, 2021, 285: 119793

33 Gong Z, Liu R, Gong H, et al. Constructing a graphene-encapsulated amorphous/crystalline heterophase NiFe alloy by microwave thermal shock for boosting the oxygen evolution reaction. ACS Catal, 2021, 11: 12284–12292

34 Yadav D K, Uma S, Nagarajan R. Microwave-assisted synthesis of ternary Li-M-Al LDHs (M = Mg, Co, Ni, Cu, Zn, and Cd) and examining their use in phenol oxidation. Appl Clay Sci, 2022, 228: 106655

35 Qiu H, Sun X, An S, et al. Microwave synthesis of histidine-functionalized graphene quantum dots/Ni-Co LDH with flower ball structure for supercapacitor. J Colloid Interface Sci, 2020, 567: 264–273

36 Liu D C, Cao L M, Luo Z M, et al. An *in situ* generated amorphous CoFePi and crystalline $Ni(PO_3)_2$ heterojunction as an efficient electrocatalyst for oxygen evolution. J Mater Chem A, 2018, 6: 24920–24927

37 He X M, Jing Y X, Wang L Q, et al. Highly stable hierarchical core-shell structure $CuMn_{0.5}Co_2O_4$@CC with self-regulating electronic and conductivity for its improved OER performance. Int J Hydrogen Energy, 2024, 51: 880–889

38 Pan T, Zhou W, Wei Q, et al. Surface-energy-regulated growth of α-phase $Cs_{0.03}FA_{0.97}PbI_3$ for highly efficient and stable inverted perovskite solar cells. Adv Mater, 2023, 35: 2208522

39 Qiao C, Zhang Y, Zhu Y, et al. One-step synthesis of zinc–cobalt layered double hydroxide (Zn–Co-LDH) nanosheets for high-efficiency oxygen evolution reaction. J Mater Chem A, 2015, 3: 6878–6883

40 Liu M, Min K, Han B, et al. Interfacing or doping? Role of Ce in highly promoted water oxidation of NiFe-layered double hydroxide. Adv Energy Mater, 2021, 11: 2101281

41 Li W, Chen S, Zhong M, et al. Synergistic coupling of NiFe layered double hydroxides with Co-C nanofibers for high-efficiency oxygen evolution reaction. Chem Eng J, 2021, 415: 128879

42 Zhang J, Dong C, Wang Z, et al. A new defect-rich CoGa layered double hydroxide as efficient and stable oxygen evolution electrocatalyst. Small Methods, 2019, 3: 1800286

43 Zhang X, Zhao Y, Zhao Y, et al. A simple synthetic strategy toward defect-rich porous monolayer NiFe-layered double hydroxide nanosheets for efficient electrocatalytic water oxidation. Adv Energy Mater, 2019, 9: 1900881

44 Xiao Z, Huang Y C, Dong C L, et al. *Operando* identification of the dynamic behavior of oxygen vacancy-rich Co_3O_4 for oxygen evolution reaction. J Am Chem Soc, 2020, 142: 12087–12095

45 Chala S A, Tsai M C, Olbasa B W, et al. Tuning dynamically formed active phases and catalytic mechanisms of *in situ* electrochemically activated layered double hydroxide for oxygen evolution reaction. ACS Nano, 2021, 15: 14996–15006

46 Zhong H, Wang X, Sun G, et al. Optimization of oxygen evolution activity by tuning e^*_g band broadening in nickel oxyhydroxide. Energy Environ Sci, 2023, 16: 641–652

补充材料

图S1 以超纯水为溶剂合成的NiFe LDH/CC的SEM和TEM图
图S2 NiMn LDH/CC的SEM、TEM和XRD图
图S3 CoFe LDH/CC的SEM、TEM和XRD图
图S4 NiCo LDH/CC的SEM、TEM和XRD图
图S5 NiFe LDH/CC-Gl的法拉第效率
图S6 不同溶剂合成的NiFe LDH/CC催化剂在1 mol L^{-1} KOH中的循环伏安曲线
图S7 水热法合成NiFe LDH/CC的SEM和XRD图
图S8 电沉积法合成NiFe LDH/CC的SEM和XRD图
图S9 不同方法合成的NiFe LDH/CC催化剂在1 mol L^{-1} KOH中的循环伏安曲线
图S10 微波法合成的NiFe LDH/CC催化剂在Laviron方程中的分析
图S11 电沉积法合成的NiFe LDH/CC催化剂在Laviron方程中的分析
图S12 水热法合成的NiFe LDH/CC催化剂在Laviron方程中的分析
表S1 NiFe LDH/CC和最近报道的一些LDHs的过电位和Tafel斜率的比较

本文以上补充材料见网络版csb.scichina.com. 补充材料为作者提供的原始数据, 作者对其学术质量和内容负责.

Summary for “微波法快速、原位合成NiFe LDH纳米片阵列用于高效电催化水氧化”

Rapid and *in-situ* synthesis of NiFe LDH nanosheet array using microwave method for efficient electrocatalytic water oxidation

Shasha Wang, Xuyun Lu, Yanan Chang, Xiaoxuan Li, Ying Liu* & Jianchun Bao*

School of Chemistry and Materials Science, Nanjing Normal University, Nanjing 210023, China
* Corresponding authors, E-mail: liuyingg@njnu.edu.cn; baojianchun@njnu.edu.cn

The complex kinetics and high energy barrier of oxygen evolution reaction (OER) seriously restrict the efficiency of hydrogen production in overall water splitting. Layered double hydroxides (LDHs) have reasonable electrocatalytic OER ability, but the resulting performance is unsatisfactory; moreover, their rapid, large-scale, and *in situ* synthesis remains a great challenge. Compared to the traditional hydrothermal, electrodeposition and co-precipitation methods, microwave synthesis methods have the advantages of cleanliness, high efficiency, and low energy consumption. Importantly, microwave methods can generate many defects to improve the electrocatalytic performance. The microwave-assisted synthesis of LDHs has been reported, but it was limited to powdered nano/micromaterials. The use of microwave methods to grow nano/microarrays *in situ* on a substrate surface has not been reported. Compared with powders, arrays have multiple advantages, such as favorable electrolyte diffusion, proton/electron transport, and direct use for electrochemical testing without the need for additional binders, so there is an urgent need to develop strategies for the *in-situ* synthesis of nano/microarrays using microwave methods. Based on these studies, this paper reports a simple and effective microwave synthesis strategy for growing layered double hydroxides arrays *in situ* on the surface of a carbon cloth (CC), termed as LDH/CC to improve the OER performance.

The type of solvent plays a crucial role in the *in situ* growth of LDHs. Compared to pure water, ethylene glycol, and pentaerythritol aqueous solvents, glycerol has a suitable polarity that can effectively regulate the surface energy of metal ions and the nucleation/migration of metal ions during the synthesis process, promoting the *in situ* and uniform growth of LDHs on the CC surface. When applied to the electrocatalytic OER, the NiFe LDH/CC catalyst synthesized using glycerol as a solvent exhibited excellent electrocatalytic performance, with a low overpotential of 257 mV (η_{100}), 279 mV (η_{200}), and 331 mV (η_{400}) at 100, 200, and 400 mA cm^{-2}, respectively. These values were superior to those for the catalyst synthesized with ethylene glycol (287, 318, and 386 mV at 100, 200, and 400 mA cm^{-2}, respectively) and pentaerythritol (309, 344, and 406 mV at 100, 200, and 400 mA cm^{-2}, respectively) as a solvent. Moreover, these performances were superior to those of many transition metal hydroxides reported in recent years.

Systematic spectroscopic and electrochemical tests have revealed that compared to traditional hydrothermal and electrodeposition methods, the NiFe LDH/CC synthesized using the microwave method shows superior characteristics. The NiFe LDH/CC prepared via microwave synthesis exhibited a uniform distribution, a high oxygen defect content, abundant electrochemical active sites, low interfacial charge transfer resistance, and high intrinsic activity. These features contribute to its outstanding performance in electrocatalytic OER applications. The NiFe LDH/CC catalyst synthesized using the microwave method displayed significantly better electrocatalytic OER performance with overpotentials of only 257 and 331 mV at 100 and 400 mA cm^{-2}, respectively. These values surpassed the performance of catalysts synthesized using hydrothermal (279 and 434 mV at 100 and 400 mA cm^{-2}, respectively) and electrodeposition methods (293 and 380 mV at 100 and 400 mA cm^{-2}, respectively). The NiFe LDH/CC catalyst also exhibited long-term electrocatalytic stability, retaining approximately 95% of its electrocatalytic OER performance after continuous operation for 100 h. The findings highlight the potential of microwave synthesis strategies for enhancing the efficiency of electrocatalytic OER processes.

This microwave synthesis strategy is not only suitable for NiFe LDH, but also for *in-situ* synthesis of NiMn LDH, CoFe LDH, and NiCo LDH, which provides a new avenue for rapid and *in-situ* synthesis of highly-active LDHs.

electrocatalytic, oxygen evolution reaction, microwave method, NiFe layered double hydroxide (LDH)

doi: 10.1360/TB-2024-0090